Desalination and Water Treatment
www.deswater.com
doi: 10.5004/dwt.2020.24952

178 (2020) 193–202
February

Adsorption of Pb(II) from aqueous solutions onto MgFeAl-CO_3 LDH: thermodynamic and kinetic studies

Abdeljalil Ait Ichou[a], Ridouan Benhiti[a], Mhamed Abali[a], Abdelkader Dabagh[a], Mohamed Chiban[a], Mohamed Zerbet[a], Gabriela Carja[b], Fouad Sinan[a,*]

[a]*Laboratory of Applied Chemistry and Environment, Department of Chemistry, Faculty of Sciences, Ibn Zohr University, BP. 8106, Hay Dakhla, Agadir, Morocco, email: f.sinan@uiz.ac.ma (F. Sinan), aitichou.contact@gmail.com (A. Ait Ichou), b.ridouan@yahoo.fr (R. Benhiti), mhamedabali@gmail.com (M. Abali), abdelkader.dabagh@gmail.com (A. Dabagh), mmchiban@yahoo.fr (M. Chiban), zerbetmohamed@gmail.com (M. Zerbet)*
[b]*Department of Chemical Engineering, Faculty of Chemical Engineering and Environmental Protection "Cristofor I. Simionescu", Technical University "Gh. Asachi" of Iasi, Bd. D. Mangeron No 71, Iasi 700554, Romania, email: carja@uaic.ro*

Received 1 September 2018; Accepted 22 September 2019

ABSTRACT

The objective of this work is to determine the kinetic and thermodynamic properties of adsorption of Pb(II) from aqueous solutions by synthetically prepared MgFeAl-CO_3 as layered double hydroxide (LDH) adsorbent. Compared to other adsorbents for heavy metal removal from aqueous solutions, LDH materials possessed many advantages such as nontoxic synthesis, chemical stability, environmentally friendly, and facile separation from the water solution. The synthesis of LDH was achieved by a co-precipitation method. The reaction products were characterized by powder X-ray diffraction, Fourier transform infrared spectroscopy, scanning electron microscopy with energy dispersive spectroscopy and N_2 sorption–desorption isotherm analysis. The adsorption rates were investigated. The effect of the parameters such as contact time, initial metal ion concentration, and temperature on the adsorption of the Pb(II) was studied. Equilibrium was achieved in 60 min and the equilibrium adsorption capacity was found to be increased with the increase in the Pb(II) initial concentration. The removal efficiency of Pb(II) increases from 59.50% to 71.15% when the temperature increases from 15°C to 60°C. The pseudo-first-order, pseudo-second-order, and Elovich kinetic models were tested and the first was found to fit better to the experimental data. The application of the intra-particle diffusion model demonstrates that the surface diffusion and the intra-particle diffusion occur in parallel during the adsorption of Pb(II) onto MgFeAl-CO_3. The equilibrium adsorption data were analyzed by Langmuir, Freundlich, Redlich–Peterson, and Temkin isotherm models. The results indicated that the Redlich–Peterson and Langmuir isotherms were the most suitable models for the obtained experimental data and the Langmuir maximum adsorption capacity of the MgFeAl-CO_3 is found to be 117.86 mg g^{-1} at 298.15 K. The thermodynamic analysis of the adsorption of Pb(II) on MgFeAl-CO_3 reveals that the present adsorption process is a spontaneous and endothermic reaction.

Keywords: LDHs; MgFeAl-CO_3; Adsorption; Lead; Kinetic; Thermodynamic

* Corresponding author.

1. Introduction

The heavy metal ions are likely to enter the drinking water and thereby damage to human health. Thus, close attention has been paid to the remediation of water contaminated by heavy metal. In addition, heavy metals are non-biodegradable, which makes it more difficult to decontaminate. Therefore, it is desirable to measure, understand, and control the heavy metal concentrations in the environment [1]. Therefore, it is necessary to find effective methods to remove the lead ions from aqueous solutions (natural water sources and industrial wastewater). There is an increasing demand for the removal of heavy metals from contaminated water to avoid ecological risk. There are many methods used for remediation of heavy metal pollution, such as ion-exchange [2], biological technologies [3], membrane filtration [4,5], solvent extraction [6], chemical precipitation [7], reverse osmosis [8], electrodialysis [9], and adsorption [10,11].

The choice of a process for the treatment of discharges depends on several factors such as the composition of the affluent, the type of reuse, the quality of the needs, etc layered double hydroxides (LDHs) can be easily synthesized and they are among the materials likely to provide a solution in the treatment of effluents, by using them as adsorbents [12].

The studied materials are mixed lamellar hydroxides of divalent metals (M^{II}) and trivalent (M^{III}). These natural or synthetic materials have been widely studied in recent years, due to their electrochemical properties [13,14], anion exchange [15] and their adsorbent potential [11,16–21], mainly related to their lamellar structure [22].

The general formula of LDHs is:

$$\left(M^{II}_{x-1}M^{III}_{x}\left(OH\right)_2\right)\left(A^{n-}_{x/n}\times yH_2O\right)$$

with $M^{II}_{x-1}\,M^{III}_{x}\,(OH)_2$ representing the layer, $A^{n-}_{x/n}\,yH_2O$ is the interlayer composition, x is the molar fraction of M^{III} per total metal, and x determines the layer charge density.

Several studies on the adsorption of anionic ions on LDHs can be found in the literature [23–26]. However, there are not many studies on the adsorption of cationic pollutants, typically cationic forms of heavy metals. Only a few LDHs phases were used as adsorbent of lead ions, e.g., CoMo [17], MgFe [27], and MgAl [28].

Recently, in literature, the adsorption processes on LDHs show an important efficiency and performance for the removal of cationic pollutants such as lead [16,17], ferrous [18], chromium [19], cadmium [20], and copper [11,21]. Based on these previous studies, more attention is concentrated on binary LDHs [16–20,28–31], while ternary LDHs that incorporate an additional metal species may offer even higher adsorption power and are rarely studied so far [21,32].

The present study focuses on the preparation and characterization of MgFeAl-CO_3 LDHs-like with a molar ratio [M^{II}/M^{III}] = 2 and aims to investigate the adsorption capacity of Pb(II) onto this LDHs in aqueous medium. The effect of contact time, initial metal ion concentrations and temperature were investigated. The experimental data were analyzed using pseudo-first-order (PFO), pseudo-second-order (PSO) and Elovich kinetic models. The Langmuir, Freundlich, Redlich–Peterson and Temkin isotherm models were used in nonlinear regression to describe equilibrium isotherms. Thermodynamic parameters like change in free energy ($\Delta G°$), enthalpy ($\Delta H°$) and entropy ($\Delta S°$) for the process of adsorption have been determined and reported.

2. Materials and methods

2.1. Adsorbent

MgFeAl-CO_3 was prepared by the co-precipitation method at constant pH [33]. A metal salt solution containing ($MgCl_2{\cdot}6H_2O$), ($FeCl_3{\cdot}6H_2O$), and ($AlCl_3{\cdot}6H_2O$) was prepared with a molar ratio [M^{II}/M^{III}] = 2. A basic solution was prepared by dissolving NaOH and Na_2CO_3 in distilled water. To achieve precipitation, the metal salt solution and basic solution were added to a vigorously stirred water. The pH of the reaction mixture was adjusted at 10 (±0.05) by the addition of concentrated NaOH solution (2 M). After that, the mixed suspension was aged for 24 h at room temperature. The resultant precipitate was collected through filtration and then washed with deionized water several times to remove soluble salts (Na_2CO_3 and NaCl) formed during the synthesis. Finally, the solid product is dried in a vacuum oven at 80°C for 10 h.

The solid structure of the adsorbent MgFeAl-CO_3 was analyzed by an X-ray diffractometer (PANalytical X'Pert Pro is a product of Malvern Panalytical, B.V. Lelyweg 1, 7602 EA Almelo, Pays-Bas). The diffractometer was operated with Cu $K_{\alpha 1}$ radiation source (λ = 1.54060 Å). Fourier transform infrared (FTIR) spectrum was obtained in 4,000–400 cm^{-1} range on an FTIR spectrometer (VERTEX 70 is a product of Bruker, Bruker Optik GmbH Rudolf-Plank-Str. 27 D-76275 Ettlingen, Germany).

2.2. Adsorbate

The stock solution of the lead ions (Pb(II)) was prepared by dissolving a pure nitrate salt for analysis $Pb(NO_3)_2$ in bidistilled water. The concentration of Pb(II) before and after adsorption was determined using an ionometer (Consort C863, Consort nv Parklaan 36 B-2300 Turnhout, Belgium) combined with a lead-specific electrode.

2.3. Batch adsorption studies

A certain amount of MgFeAl-CO_3 was added to the solution with the C_0 concentration of Pb(II), and the resultant suspension was kept stirring at 25°C. Samples were taken at different contact times and then centrifuged at 500 rpm and analyzed. The ration mass/volume (W/V) used in this study corresponds to the smallest mass of MgFeAl-CO_3 which leads to a maximum adsorption rate. This ratio was determined in our previous work with W/V = 1.75 g L^{-1} [11].

The Pb(II) removal efficiency R(%) and the amount of equilibrium adsorption q_e (mg g^{-1}) were calculated using the following two formulas:

$$R\left(\%\right)=\frac{C_0-C_t}{C_0}\times 100\% \tag{1}$$

$$q_e=\left(C_0-C_e\right)\frac{V}{W} \tag{2}$$

where C_0 and C_t are the initial and the residual concentration of Pb(II) ions at time t = 0 and t, in mg L^{-1}, respectively. C_e (mg L^{-1}) is the equilibrium concentration of Pb(II) ions, V(L) is the volume of the solution and W(g) is the mass of MgFeAl-CO_3.

3. Results and discussion

3.1. Characterization of MgFeAl-CO_3

Fig. 1 shows the X-ray diffraction (XRD) patterns of MgFeAl-CO_3. The XRD patterns exhibit sharp and symmetric reflections for the (003), (006), (113), and (110) planes and broad symmetric peaks (012), (015), and (018) planes, which are characteristics of these materials [22]. The basal spacing (d_{003}) of MgFeAl-CO_3 is 0.77 nm, which agrees well with values reported by other authors of an LDH solid bearing intercalated carbonate (~0.765 nm) [12,33].

The FTIR spectra for MgFeAl-CO_3 (Fig. 2) showed a broad and strong band at 3,430.7 cm^{-1} in the range of 3,200–3,600 cm^{-1} which was due to the O–H stretching vibration $\upsilon(OH_{str})$ of the inorganic layers (Metal-OH) and interlayer water molecules (H–OH). Another common wave number for LDH-like material is a band at 1,640.7 cm^{-1} which is assigned to the bending vibration of interlayer water molecules (H_2O). The sharp intense band at 1,359.8 is the antisymmetric stretching of interlayer carbonate $\upsilon_{as}(CO_3^{2-})$, which may be introduced into the interlayer of MgFeAl-CO_3 by absorption of CO_2 during the preparation procedure [34]. The bands between 400 and 800 cm^{-1} are attributed to the characteristic lattice vibrations of M–O.

The morphology of the synthesized LDH was investigated by scanning electron microscopy (SEM) using a scanning electron microscope (TESCAN VEGA3, TESCAN ORSAY HOLDING, a.s. Libušina tř. 21 623 00 Brno - Kohoutovice Czech Republic) with an energy dispersive spectroscopy (EDS) attachment. The accelerating voltage applied was 25 kV.

Fig. 3 shows the post-adsorption SEM images for the as-prepared LDH compound. It is seen that compounds appear as irregular aggregates of individual particles. The crystallites are barely observed and the sample was presumably present a flaky aspect. In addition, the SEM images show coverage of available pores on the surface of the synthesized LDH.

As shown in Fig. 4, the EDS pattern shows that the molar ratio of Mg/(Fe + Al) is 1.6, which was slightly lower than the theoretical ratio of 2. This result indicates that the surface of the synthesized LDH contains a much higher proportion of iron (Fe^{III}) relative to aluminum (Al^{III}), with a Fe/Al ratio of 1.52. The analysis also confirms the presence of a small amount of sodium on the material surface (0.70%), which indicates the effectiveness of the post-synthesis washing treatment. Stoichiometric compositions obtained by EDS analysis were $Mg_{0.62}Fe_{0.23}Al_{0.15}(OH)_2(CO_3)_{0.19}$, $y(H_2O)$, for MgFeAl-LDH. Cation's contents are measured by EDS and all others are calculated.

The nitrogen adsorption–desorption measurements at 77 K yielded a Type IV isotherm (Fig. 5a) with a H3-type hysteresis loop at high relative pressures (P/P^0 > 0.45–0.90), indicating that the condensation of nitrogen within the pores of the synthesized LDH and its release at reduced pressures followed different paths; a characteristic of mesoporous materials [35]. The specific surface area of 80.77 m^2 g^{-1} (Fig. 5b) with a broad pore width of 37.53 Å could be determined for the synthesized LDH (Fig. 5c). The MgFeAl-CO_3 LDH is dominated by both mesopores having diameters in the range of 2–5 nm.

3.2. Adsorption of Pb(II) onto MgFeAl-CO_3

3.2.1. Effect of contact time and kinetics modeling

Adsorption experiments for the kinetics study were conducted using a solution having 100 mg L^{-1} of initial Pb(II) concentration with an adsorbent dosage of 1.75 g L^{-1}. Throughout the study, the contact time was varied from 5 to 180 min at 25°C and the initial pH of the solution (5.45).

Fig. 6 shows that the adsorption of Pb(II) onto MgFeAl-CO_3 was increased with increasing contact time and reached equilibrium at about 60 min. The maximum removal efficiency of Pb(II) was about 64% obtained at 180 min. The pH is relatively stable between 5.5 and 6 and therefore remains below the pH value of precipitation of lead hydroxide

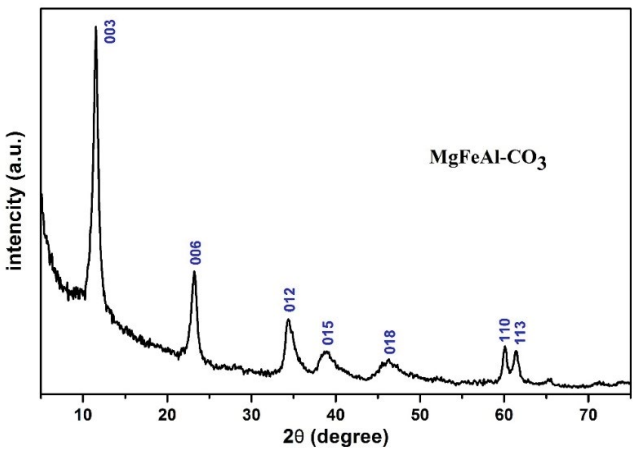

Fig. 1. XRD patterns of MgFeAl-CO_3.

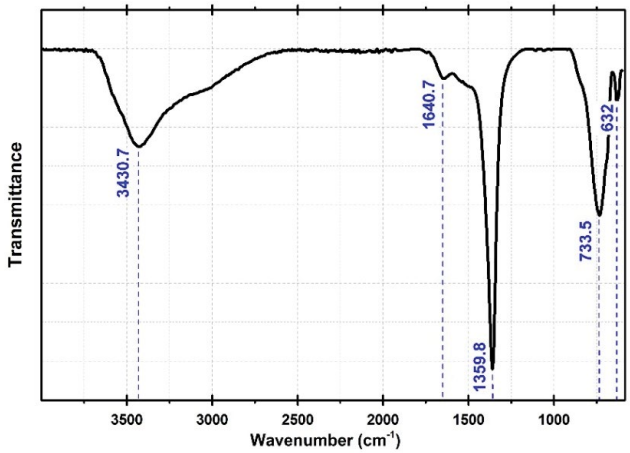

Fig. 2. FTIR spectra of MgFeAl-CO_3.

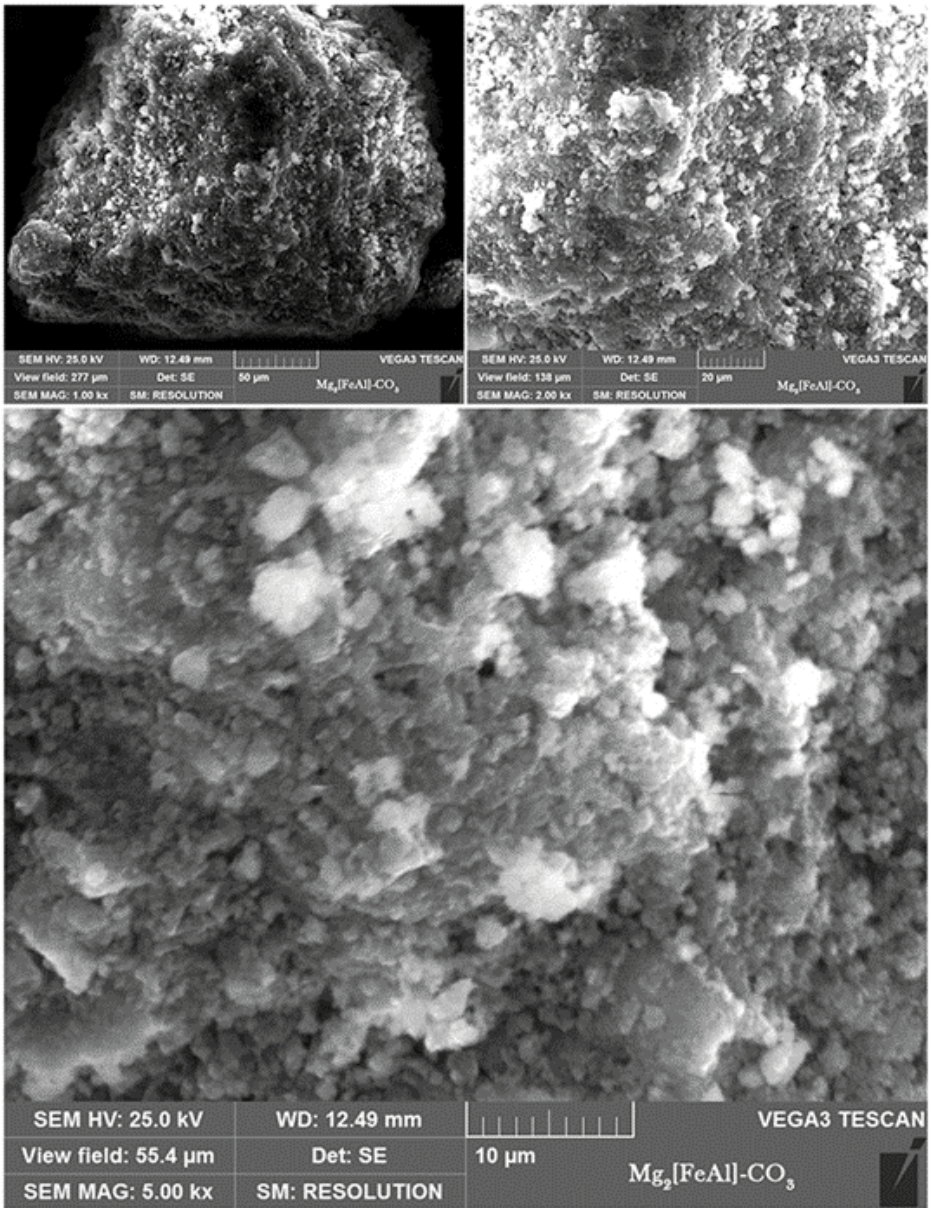

Fig. 3. SEM micrographs of the synthesized LDH.

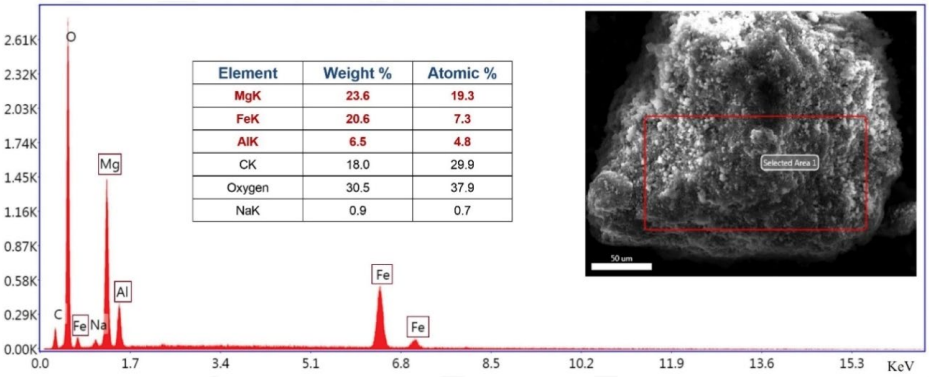

Fig. 4. EDS analysis of the synthesized LDH.

[36]. Similar results have been previously obtained using MgAl–CO_3 as adsorbent of Cd(II) [20].

Adsorption kinetic models are used to explain the adsorption mechanism and adsorption characteristics of synthesized LDH. Lagergren's PFO [37], Ho's PSO [38] and Elovich kinetic models [39], which were in nonlinear form, were applied to the experimental data. The adsorption kinetic uptake for Pb(II) by MgFeAl-CO_3 LDH was analyzed by the orthogonal distance regression algorithm using the OriginPro 9.1® software. The PFO, PSO and Elovich models are presented as follows:

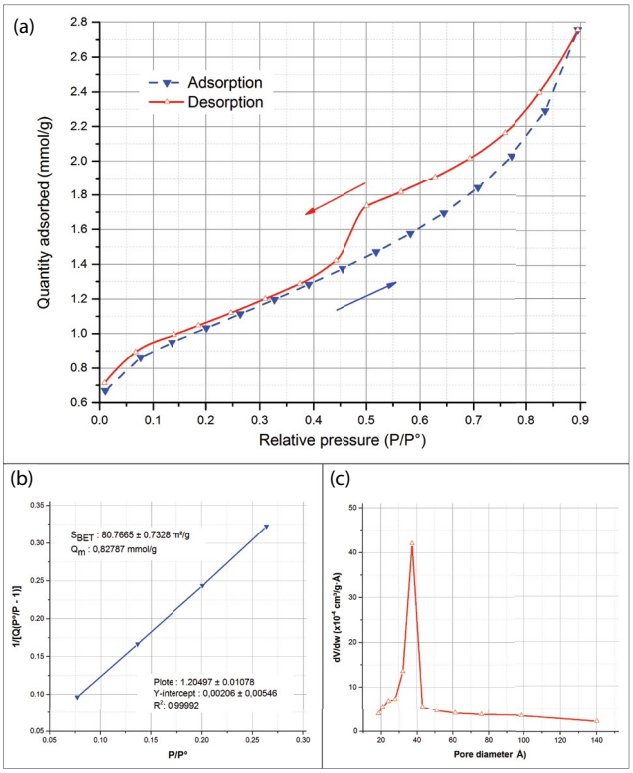

Fig. 5. (a) N_2 adsorption–desorption isotherm, (b) determination of surface area S_{BET} ($0.05 < P/P^0 < 0.30$), and (c) pore size distribution curve of MgFeAl-CO_3 synthesized.

Pseudo-first-order kinetic model:

$$q_t = q_e\left(1 - e^{-k_1 t}\right) \tag{3}$$

Pseudo-second-order kinetic model:

$$q_t = \frac{k_2 q_e^2 t}{\left(1 + k_2 q_e t\right)} \tag{4}$$

Elovich kinetic model:

$$q_t = \frac{1}{\beta}\ln\left(\alpha\beta\right) + \frac{1}{\beta}\ln\left(t\right) \tag{5}$$

where q_t is the adsorption capacity of Pb(II) (mg g^{-1}) at time t (min), q_e is the adsorption capacity of Pb(II) (mg g^{-1}) at equilibrium, k_1 is the PFO model rate constant (min^{-1}), k_2 is the PSO model rate constant (g mg^{-1} min^{-1}), α and β, known as the Elovich coefficients. The α represents the initial adsorption rate (mg g^{-1} min^{-1}) and β is the desorption constant (g mg).

Nonlinear kinetic models of PFO, PSO, and Elovich plots are all described in Fig. 7.

The adsorption rate constants (k_1 and k_2), the equilibrium adsorption capacities calculated from the PFO and PSO model ($q_{e,cal}$), the Elovich coefficients (α and β), the correlation coefficient (R^2) and Chi-square value (χ^2) for each system were calculated according to the nonlinear regression analyses. The corresponding values of kinetics parameters are presented in Table 1. For the entire adsorption process, it can be seen that the PFO kinetic model gave the highest R^2 (0.9999) and lowest χ^2 values (lesser than 0.5) compared to the PSO and the Elovich model. The kinetic data generated from the PFO model fitted the experimental data reasonably well and the calculated $q_{e,cal}$ value (36.59 mg g^{-1}) is very close to the experimental $q_{e,exp}$ value (36.46 mg g^{-1}). However, the Elovich model shows poor-fitting with the experimental data and the highest χ^2 values (9.539). Thus, the PFO kinetic model is much better than the PSO and Elovich models in interpreting the adsorption of Pb(II) onto MgFeAl-CO_3.

During adsorption processes, the solute transfer is usually characterized by external mass transfer (boundary layer diffusion), intra-particle diffusion or both. We can

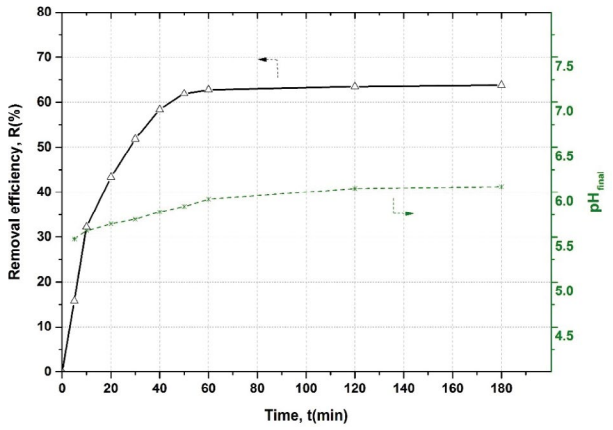

Fig. 6. Effect of contact time on Pb(II) adsorption onto MgFeAl-CO_3.

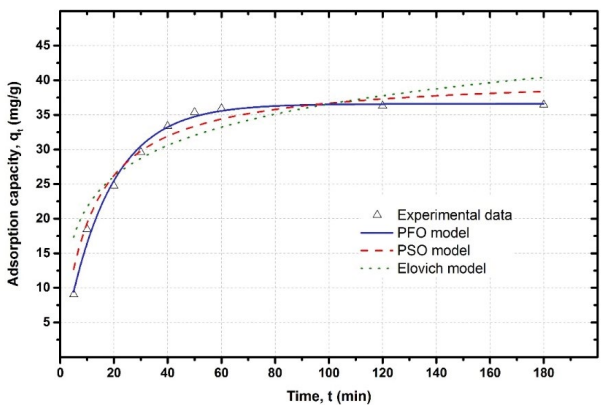

Fig. 7. Nonlinear kinetic models for adsorption of Pb(II) onto MgFeAl-CO_3.

Table 1
Kinetic parameters of PFO, PSO, and Elovich models for Pb(II) adsorption onto MgFeAl-CO_3

PFO		PSO		Elovich	
$q_{e,cal}$ (mg g^{-1})	36.588	$q_{e,cal}$ (mg g^{-1})	40.739	α (mg g^{-1} min^{-1})	17.108
k_1 (min^{-1})	0.0597	k_2 (g mg^{-1} min^{-1})	0.0022	β (g mg^{-1})	0.1522
R^2	0.9999	R^2	0.9994	R^2	0.9978
χ^2	0.4928	χ^2	2.5743	χ^2	9.5390

fit an intra-particle diffusion plot to identify the adsorption mechanism. This model based on the theory proposed by Weber and Morris was used to identify the diffusion mechanism as well [40]:

$$q_t = k_{Di} t^{\frac{1}{2}} + C_i \quad (6)$$

where k_{Di} is the intra-particle diffusion rate constant of stage i (mg g^{-1} $min^{-1/2}$), and C_i is the intercept of stage i, and it provides information on the thickness of the boundary layer. If the intra-particle diffusion model is valid, the amount of adsorbate uptake q_t vs. $t^{1/2}$ would result in a linear relationship. C_i and k_i values can be obtained from these plots.

For Pb(II) adsorption onto MgFeAl-CO_3, a plot of q_t vs. $t^{1/2}$ gives three distinct regimes (Fig. 8), which can be fitted by straight lines. The first stage in diffusion model is the mass transfer of adsorbate molecule from the aqueous solution to the adsorbent surface (surface or film diffusion), the second stage is a progressive adsorption where there is a limitation of the velocity due to the intra-particle diffusion (intra-particle or pore diffusion) and the last is relative to the equilibrium [40].

Table 2 shows the parameters estimated by fitting the intra-particle diffusion model to the kinetic data of Pb(II) adsorption onto MgFeAl-CO_3. It can be noticed that the intra-particle diffusion rate constants, k_{D1} (9,123 mg g^{-1} $min^{-1/2}$), for the first adsorption step are higher than k_{D2} (0.965 mg g^{-1} $min^{-1/2}$), indicating that the adsorption rate was higher at the beginning and decreased over time. However, the straight lines for both plots did not intersect

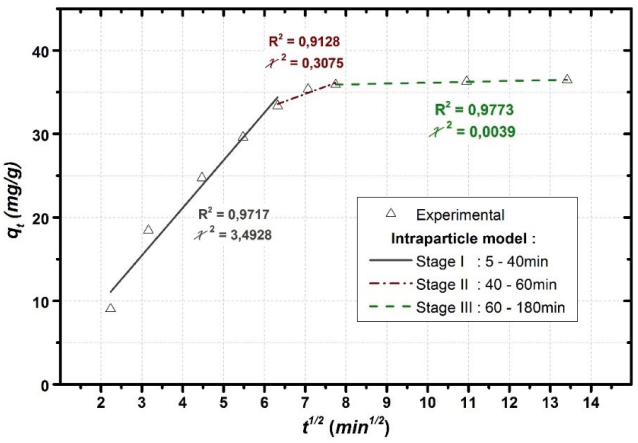

Fig. 8. Intra-particle diffusion plots for Pb(II) adsorption onto MgFeAl-CO_3 at 25°C.

Table 2
Parameter values for intra-particle diffusion model for Pb(II) adsorption

Stage I (surface or film diffusion)		Stage II (intra-particle or pore diffusion)		Stage III (final equilibrium)	
k_{D1}	C_1	k_{D2}	C_2	k_{D3}	C_3
9.123	–5.211	0.965	44.42	0.091	51.19

the origin (C_1 and $C_2 \neq 0$) suggesting surface diffusion and pore diffusion are controlling the adsorption of Pb(II) onto MgFeAl-CO_3. Similar kind of observable facts was reported by other researchers [40–42]. Furthermore, the hydrated radius of Pb(II) is about 0.401 nm [43], which is very smaller than the average pore diameter of the MgFeAl-CO_3 (3.753 nm). In this case, the diffusion of Pb(II) into the pore space of the LDH should be possible.

k_{Di} is the intra-particle diffusion rate constant of stage i in mg g^{-1} $min^{-1/2}$

3.2.2. Effect of initial concentration and isotherm modeling

The equilibrium adsorption capacity is highly dependent on the initial concentration (C_i) of the solution of adsorbate. For the evaluation of the effect of initial concentration, 40 mL solution of different initial concentrations of Pb(II) was treated onto the adsorbent. Initial concentration was varied from 10 to 300 mg L^{-1}. The study results are illustrated in Fig. 9. It shows that Pb(II) adsorption capacity was increased with increasing of initial concentrations. With the increase of Pb(II) concentration, the opportunity for binding sites to entrap Pb(II) is increased; thus, the adsorption capacity is increased. The highest Pb(II) adsorption capacity (q_e = 78.54 mg g^{-1}) was achieved at an initial concentration of 300 mg L^{-1}.

The adsorption isotherms of Pb(II) on MgFeAl-CO_3 are illustrated in Fig. 10. Langmuir isotherm [44], Freundlich isotherm [45], Redlich–Peterson isotherm [46] and Temkin isotherm [47] was applied to fit the experimental data. These nonlinear isotherms are presented as follows:

Langmuir isotherm model:

$$q_e = \frac{q_m K_L C_e}{1 + K_L C_e} \quad (7)$$

Freundlich isotherm model:

$$q_e = K_F C_e^n \quad (8)$$

Redlich–Peterson isotherm model:

$$q_e = \frac{K_{R-P} C_e}{1 + \alpha_{R-P} C_e^{\beta}} \tag{9}$$

Temkin isotherm model:

$$q_e = \frac{RT}{b} \ln\left(K_T C_e\right) \tag{10}$$

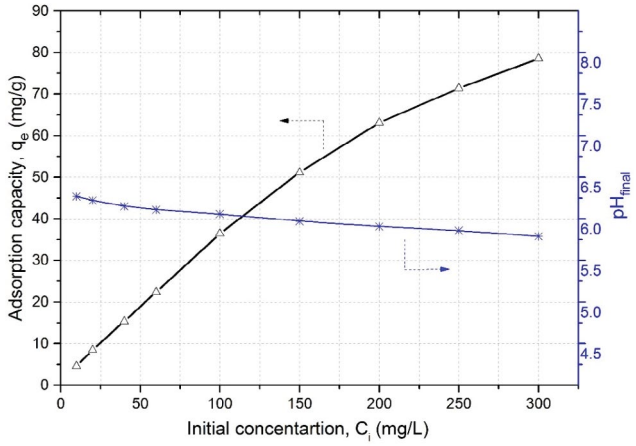

Fig. 9. Effect of initial concentration on the adsorption of Pb(II) ions by MgFeAl-CO_3. (conditions: W/V = 1.75 g L^{-1}, t_c = 180 min, pH_i = 5.45, T = 25°C).

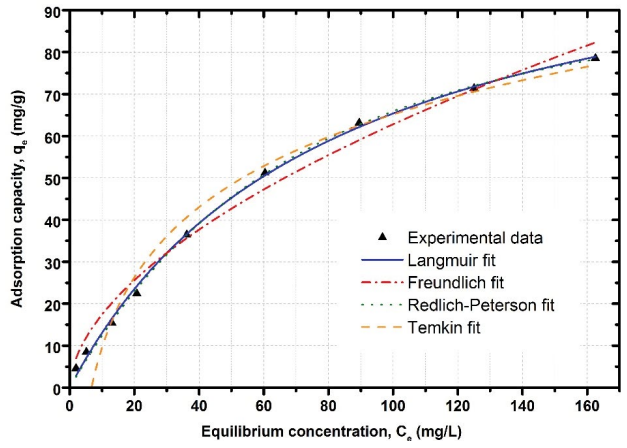

Fig. 10. Nonlinear plots for the adsorption isotherms of Pb(II) ions by MgFeAl-CO_3.

where q_e is the adsorption capacity of Pb(II) (mg g^{-1}) at equilibrium, C_e (mg L^{-1}) is concentration of Pb(II) in aqueous solution at equilibrium, q_m is the maximum adsorption capacity of Pb(II) in theory, and K_L is Langmuir constant (L mg^{-1}), K_F is Freundlich constant (L^n g^{-1} mg^{n-1}), n is heterogeneity factor, K_{R-P} is Redlich–Peterson constant (L g^{-1}), α_{R-P} is constant (L $mg^{-1})^{-\beta}$, β is exponent that lies between 0 and 1, R is gas constant (8.314 J mol^{-1} K^{-1}), T is temperature (K), b is Temkin constant which is related to the heat of sorption (J mol^{-1}), and K_T is Temkin isotherm constant (L g^{-1}).

The unknown parameters of the isotherm models were determined by nonlinear regression (orthogonal distance regression algorithm) using OriginPro 9.1® software [48]. All calculated model parameters are presented in Table 3. The Langmuir isotherm model is representative of monolayer adsorption and assumes that the solid surface has a finite number of identical sites that show homogeneous surfaces [44]. Freundlich isotherm indicates non-ideal and reversible adsorption, not restricted to the formation of monolayer [49]. Redlich–Peterson isotherm is widely used as a compromise between the Langmuir and Freundlich systems and which can be applied either homogeneous or heterogeneous systems due to its versatility; therefore the mechanism of adsorption is a mix and does not follow ideal monolayer adsorption [46,47]. Temkin isotherm contains a factor that explicitly takes into account the interactions between adsorbent and adsorbate. In this isotherm, it is assumed that the heat of adsorption of all molecules decreases when the surface of the adsorbent is more covered [50].

Based on the R^2 and χ^2 values (Table 3), the Redlich–Peterson isotherm model was a better fit with the adsorption of Pb(II) onto the MgFeAl-CO_3 than Langmuir, Freundlich and Temkin models. It was determined that best-fitted adsorption isotherm models were obtained to be in the order: Redlich–Peterson > Langmuir > Freundlich > Temkin isotherms. The Redlich–Peterson isotherm exhibited the highest R^2 and the lowest χ^2 values (R^2 = 0.99983 and χ^2 = 0.71788) same as Langmuir isotherm (R^2 = 0.99981 and χ^2 = 0.80465), which provided a considerably better fit as compared to Freundlich and Temkin but similar to the Langmuir isotherm. It can also be observed that the value of β is more than unity (β = 1.12251), which means the isotherms are approaching the Langmuir and not the Freundlich. Generally, the value of β lies between 0 and 1 but an adsorption model could be referred to as the Langmuir isotherm model when β ≥ 1 [51,52]. In this study, the β value thus confirms the adsorption mechanism to be a hybrid one, preferentially following the ideal monolayer adsorption coverage characteristics of

Table 3
Parameters of the Langmuir, Freundlich, Redlich–Peterson and Temkin isotherms

Langmuir		Freundlich		Redlich–Peterson		Temkin	
q_m (mg g^{-1})	117.864	n	0.55717	α_{R-P} (L $mg^{-1})^{-\beta}$	0.00586	b_T (J mol^{-1})	24.1612
K_L (L mg^{-1})	0.01246	K_F (Ln g^{-1} mg^{n-1})	4.82644	K_{R-P} (L g–1)	1.33758	K_T (L g–1)	0.14830
R^2	0.99981	R^2	0.99771	R^2	0.99983	R^2	0.99734
χ^2	0.80465	χ^2	9.71584	χ^2	0.71788	χ^2	11.2945
–	–	–	–	β	1.12251	–	–

the Langmuir model with the predicted maximum capacity of adsorption (q_m) value of about 117.86 mg g^{-1}. Thus, it can be concluded that Redlich–Peterson and Langmuir isotherms were the most suitable models for the adsorption of Pb(II) onto MgFeAl-CO_3. Other researchers have reported similar findings as well [53–55].

3.2.3. Effect of temperature and thermodynamics study

The effect of temperature on adsorption of Pb(II) onto MgFeAl-CO_3 is conducted at a range of 15°C to 60°C. Results presented in Fig. 11 show that the removal efficiency of Pb(II) increases significantly with the increase in temperature from 288.15 (59.50%) to 333.15 K (71.15%), indicating that the adsorption process is endothermic. This shows an increase in the feasibility of Pb(II) adsorption at higher temperatures, which might be because of the higher temperatures cause the diffusion of Pb(II) molecules from the solution to the adsorbent to be faster [50]. This is also to be attributed to either change in pore size of the adsorbent improving intra-particle diffusion within the pores or enhancement in the chemical affinity of Pb(II) ions to the surface of the adsorbent [56].

To describe the thermodynamic behavior of the adsorption of Pb(II) on the MgFeAl-CO_3, three thermodynamic parameters were studied: the Gibbs free energy ($\Delta G°$), the enthalpy change ($\Delta H°$), and the entropy change ($\Delta S°$). The $\Delta G°$ values were calculated from the following equation [57]:

$$\Delta G^{\circ} = -RT\ln\left(1{,}000K_d\right) \tag{11}$$

where R is the universal gas constant (8.314 J mol^{-1} K^{-1}), T is the temperature (K) and K_d is the distribution coefficient.

The K_d value was calculated using the following equation:

$$K_d = \frac{q_e}{C_e} \tag{12}$$

where q_e and C_e are the equilibrium concentration of Pb(II) on MgFeAl-CO_3 (mg g^{-1}) and in the solution (mg L^{-1}), respectively.

The $\Delta H°$ and $\Delta S°$ of adsorption were estimated from the following equation:

$$\ln\left(1{,}000K_d\right) = \frac{\Delta S°}{R} - \frac{\Delta H°}{RT} \tag{13}$$

According to equation (13), $\Delta H°$ and $\Delta S°$ parameters can be calculated from the slope and intercept of the plot of Ln(1,000 K_d) vs. 1/T, respectively (Fig. 12).

The corresponding values of all thermodynamic parameters are given in Table 4. This shows that $\Delta G°$ is negative at temperatures greater than or equal to 298 K. The negative $\Delta G°$ values indicated that thermodynamically spontaneous

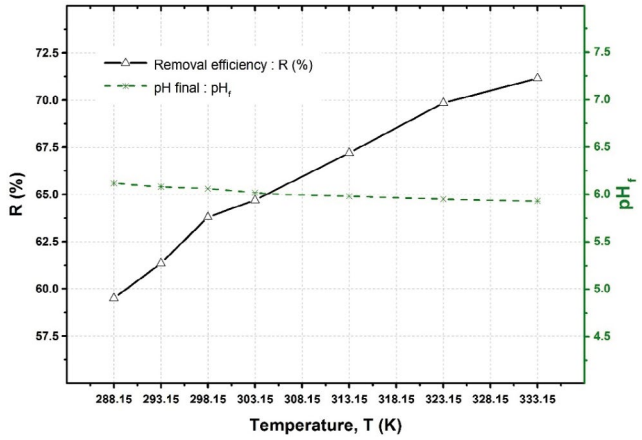

Fig. 11. Effect of temperature on adsorption of Pb(II) onto MgFeAl-CO_3.

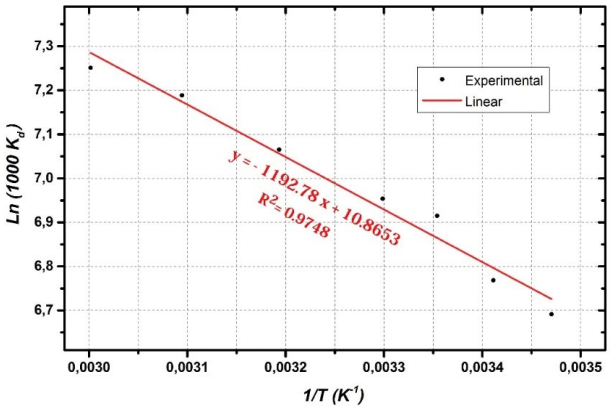

Fig. 12. Plot of Ln(1,000 K_d) vs. 1/T for estimation of thermodynamic parameters for the adsorption of Pb(II) on MgFeAl-CO_3.

Table 4
Thermodynamic parameters for the adsorption of Pb(II) onto MgFeAl-CO_3 as a function of temperature

T (K)	K_d	$\Delta G°$ (kJ mol^{-1})	$\Delta H°$ (kJ mol^{-1})	$\Delta S°$ (J mol^{-1} K^{-1})	R^2
288	0.8055	–16.03			
293	0.8698	–16.50			
298	1.0071	–17.14			
303	1.0473	–17.53	9.955	90.334	0.9748
313	1.1707	–18.39			
323	1.3239	–19.31			
333	1.4093	–20.08			

nature of the adsorption process. In addition, the decrease in $\Delta G°$ values with an increase in temperature shows that the adsorption process was relatively favorable at higher temperatures [58]. The positive values of $\Delta H°$ (9.955 kJ mol^{-1}) implies that the adsorption process was endothermic. The positive values of $\Delta S°$ (90.334 J mol^{-1} K^{-1}) shows the increased disorder and randomness at the solid-solution interface [59].

4. Conclusion

In the present work, the kinetics and thermodynamics of the adsorption of Pb(II) onto MgFeAl-CO_3 were studied. The obtained results indicate that MgFeAl-CO_3 is an effective adsorbent for Pb(II) from aqueous solutions.

The MgFeAl-CO_3 used in this study was synthesized using the co-precipitation method at constant pH. The results of XRD and FTIR characterization confirmed that the material obtained, corresponding to the LDH-like compounds intercalated with carbonate ions. The results of SEM analysis indicated that the LDH synthesized appeared as irregular aggregates of individual particles and show coverage of available pores on the surface. The surface of MgFeAl-CO_3 synthesized was mesoporous, with Brunauer–Emmett–Teller surface area close to 81 m^2 g^{-1}.

The ability of MgFeAl-CO_3 to adsorb Pb(II) ions from aqueous solution was investigated. The effects of contact time, initial metal ion concentrations and temperature were considered. The adsorption equilibrium was reached after 60 min. The removal efficiency of Pb(II) was greatly increased with an increase in initial concentration and temperature. By applying the kinetic models to the experimental data, it was found that the kinetics of Pb(II) adsorption onto MgFeAl-CO_3 followed the PFO rate equation (R^2 value close to unity and χ^2 value less than 0.5). Fitting the data to the intra-particle diffusion model, suggesting that the surface adsorption and intra-particle diffusion were concurrently operating. Redlich–Peterson and Langmuir isotherms were the most suitable models for the adsorption of Pb(II) onto MgFeAl-CO_3. These results indicated that the adsorption mechanism is a hybrid one, preferentially following the ideal monolayer adsorption coverage characteristics of the Langmuir model, with maximum adsorption capacity value of 117.86 mg g^{-1}. The calculated thermodynamic parameters indicated the endothermic ($\Delta H° > 0$) and spontaneous nature ($\Delta G° < 0$) of the adsorption process in the temperature range of 288–333 K.

References

[1] J.P. Chen, Decontamination of Heavy Metals: Processes, Mechanisms, and Applications, CRC Press, Florida, 2012.

[2] A. Bashir, L.A. Malik, S. Ahad, T. Manzoor, M.A. Bhat, G.N. Dar, A.H. Pandith, Removal of heavy metal ions from aqueous system by ion-exchange and biosorption methods, Environ. Chem. Lett., 17 (2019) 729–754.

[3] S. Ye, G. Zeng, H. Wu, C. Zhang, J. Dai, J. Liang, J. Yu, X. Ren, H. Yi, M. Cheng, C. Zhang, Biological technologies for the remediation of co-contaminated soil, Crit. Rev. Biotechnol., 37 (2017) 1062–1076.

[4] C. Fersi Bennani, O. M'hiri, Comparative study of the removal of heavy metals by two nanofiltration membranes, Desal. Wat. Treat., 53 (2015) 1024–1030.

[5] Y.-R. Qiu, L.-J. Mao, Removal of heavy metal ions from aqueous solution by ultrafiltration assisted with copolymer of maleic acid and acrylic acid, Desalination, 329 (2013) 78–85.

[6] B. Fetouhi, H. Belarbi, A. Benabdellah, S. Kasmi-Mir, G. Kirsch, Extraction of the heavy metals from the aqueous phase in ionic liquid 1-butyl-3-methylimidazolium hexafluorophosphate by N-salicylideneaniline, J. Mater. Environ. Sci., 7 (2016) 746–754.

[7] M.M. Brbooti, B.A. Abid, N.M. Al-Shuwaiki, Removal of heavy metals using chemicals precipitation, English Technol. J., 29 (2011) 595–612.

[8] S.A. Al-Jlil, O.A. Alharbi, Comparative study on the use of reverse osmosis and adsorption process for heavy metals removal from wastewater in Saudi Arabia, Res. J. Environ. Sci., 4 (2010) 400–406.

[9] E. Aytaç, S. Altın, Influence of flow rate on the removal of copper, lead and nickel from solutions in electrodialysis process, MATTER: Int. J. Sci. Technol., 3 (2017) 24–35.

[10] M. Chiban, A. Soudani, F. Sinan, M. Persin, Single, binary and multi-component adsorption of some anions and heavy metals on environmentally friendly *Carpobrotus edulis* plant, Colloids Surf., B, 82 (2011) 267–276.

[11] A. Ait Ichou, M. Abali, M. Chiban, G. Carja, M. Zerbet, E. Eddaoudi, F. Sinan, Élaboration et caractérisation d'argiles synthétiques de type HDL et leur application pour l'adsorption des ions Cu^{2+} (Development and characterization of synthetic clay LDH type and their application on the adsorption of Cu^{2+} ions), J. Mater. Environ. Sci., 5 (2014) 2444–2448.

[12] M.Á. Ulibarri, M. del C. Hermosín, Layered Double Hydroxides in Water Decontamination, V. Rives, Ed., Layered Double Hydroxides: Present and Future, Nova Science Publishers, New York U.S.A., 2006, pp. 285–321.

[13] L. Lei, M. Hu, X. Gao, Y.M. Sun, The effect of the interlayer anions on the electrochemical performance of layered double hydroxide electrode materials, Electrochim. Acta, 54 (2008) 671–676.

[14] M.F. Shao, R.K. Zhang, Z.H. Li, M. Wei, D.G. Evans, X. Duan, Layered double hydroxides toward electrochemical energy storage and conversion: design, synthesis and applications, Chem. Commun., 51 (2015) 15880–15893.

[15] L. El Gaini, M. Lakraimi, E. Sebbar, A. Meghea, M. Bakasse, Removal of indigo carmine dye from water to Mg–Al–CO_3-calcined layered double hydroxides, J. Hazard. Mater., 161 (2009) 627–632.

[16] Y. Yasin, M. Mohamad, A. Saad, A. Sanusi, F.H. Ahmad, Removal of lead ions from aqueous solutions using intercalated tartrate-Mg–Al layered double hydroxides, Desal. Wat. Treat., 52 (2014) 4266–4272.

[17] M.S. Mostafa, A.-S.A. Bakr, A.M.A. El Naggar, E.-S.A. Sultan, Water decontamination via the removal of Pb (II) using a new generation of highly energetic surface nano-material: $Co^{(+2)}$ $Mo^{(+6)}$ LDH, J. Colloid Interface Sci., 461 (2016) 261–272.

[18] A.A. Bakr, M.S. Mostafa, G. Eshaq, M.M. Kamel, Kinetics of uptake of Fe(II) from aqueous solutions by Co/Mo layered double hydroxide (Part 2), Desal. Wat. Treat., 56 (2015) 248–255.

[19] T. Kameda, E. Kondo, T. Yoshioka, Treatment of Cr(VI) in aqueous solution by Ni–Al and Co–Al layered double hydroxides: equilibrium and kinetic studies, J. Water Process Eng., 8 (2015) e75–e80.

[20] R. Shan, L. Yan, K. Yang, Y. Hao, B. Du, Adsorption of Cd(II) by Mg–Al–CO_3^- and magnetic Fe_3O_4/Mg–Al–CO_3-layered double hydroxides: kinetic, isothermal, thermodynamic and mechanistic studies, J. Hazard. Mater., 299 (2015) 42–49.

[21] A.A. Bakr, G. Eshaq, A.M. Rabie, A.H. Mady, A.E. El Metwally, Copper ions removal from aqueous solutions by novel Ca–Al–Zn layered double hydroxides, Desal. Wat. Treat., 57 (2016) 12632–12643.

[22] D.G. Evans, R.C.T. Slade, Structural Aspects of Layered Double Hydroxides, in: Structure and Bonding, Springer-Verlag, Berlin/Heidelberg, 2006, pp. 1–87.

[23] K.-H. Goh, T.-T. Lim, Z. Dong, Application of layered double hydroxides for removal of oxyanions: a review, Water Res., 42 (2008) 1343–1368.

[24] D. Chaara, I. Pavlovic, F. Bruna, M.A. Ulibarri, K. Draoui, C. Barriga, Removal of nitrophenol pesticides from aqueous solutions by layered double hydroxides and their calcined products, Appl. Clay Sci., 50 (2010) 292–298.
[25] F.L. Theiss, S.J. Couperthwaite, G.A. Ayoko, R.L. Frost, A review of the removal of anions and oxyanions of the halogen elements from aqueous solution by layered double hydroxides, J. Colloid Interface Sci., 417 (2014) 356–368.
[26] Y. Xu, S. Guo, W. Xia, L. Dou, J. Zhou, J. Zhang, J. Liu, G. Qian, Removal competition mechanism of orthophosphate and pyrophosphate by CaFe-Cl-LDHs, Desal. Wat. Treat., 57 (2016) 29393–29403.
[27] X. Liang, W. Hou, J. Xu, Sorption of Pb(II) on Mg-Fe layered double hydroxide, Chin. J. Chem., 27 (2009) 1981–1988.
[28] M.A. González, I. Pavlovic, C. Barriga, Cu(II), Pb(II) and Cd(II) sorption on different layered double hydroxides. A kinetic and thermodynamic study and competing factors, Chem. Eng. J., 269 (2015) 221–228.
[29] L. Ma, Q. Wang, S.M. Islam, Y. Liu, S. Ma, M.G. Kanatzidis, Highly selective and efficient removal of heavy metals by layered double hydroxide intercalated with the MoS_4^{2-} ion, J. Am. Chem. Soc., 138 (2016) 2858–2866.
[30] N. Ayawei, C.Y. Abasi, D. Wankasi, E.D. Dikio, Layered double hydroxide adsorption of lead: equilibrium, thermodynamic and kinetic studies, Int. J. Adv. Res. Chem. Sci., 2 (2015) 22–32.
[31] X. He, X. Qiu, C. Hu, Y. Liu, Treatment of heavy metal ions in wastewater using layered double hydroxides: a review, J. Dispersion Sci. Technol., 39 (2018) 792–801.
[32] S.-S. Li, M. Jiang, T.-J. Jiang, J.-H. Liu, Z. Guo, X.-J. Huang, Competitive adsorption behavior toward metal ions on nano-Fe/Mg/Ni ternary layered double hydroxide proved by XPS: evidence of selective and sensitive detection of Pb(II), J. Hazard. Mater., 338 (2017) 1–10.
[33] F. Cavani, F. Trifirò, A. Vaccari, Hydrotalcite-type anionic clays: preparation, properties and applications, Catal. Today, 11 (1991) 173–301.
[34] J. He, M. Wei, B. Li, Y. Kang, D.G. Evans, X. Duan, Preparation of Layered Double Hydroxides, in: Layered Double Hydroxides, Springer-Verlag, Berlin/Heidelberg, 2005, pp. 89–119.
[35] K.S.W. Sing, D.H. Everett, R.A.W. Haul, L. Moscou, R.A. Pierotti, J. Rouquerol, T. Siemieniewska, Reporting Physisorption Data for Gas/Solid Systems, in: Handbook of Heterogeneous Catalysis, Wiley-VCH Verlag GmbH & Co. KGaA, Weinheim, Germany, 2008, pp. 1217–1230.
[36] R. Escudero, E. Espinoza, F.J. Tavera, Precipitation of lead species in a Pb–H_2O system, Res. J. Recent Sci., 2 (2013) 1–4.
[37] Y.-S. Ho, Citation review of Lagergren kinetic rate equation on adsorption reactions, Scientometrics, 59 (2004) 171–177.
[38] Y.-S. Ho, Review of second-order models for adsorption systems, J. Hazard. Mater., 136 (2006) 681–689.
[39] S. Vahidhabanu, D. Karuppasamy, A.I. Adeogun, B.R. Babu, Impregnation of zinc oxide modified clay over alginate beads: a novel material for the effective removal of congo red from wastewater, RSC Adv., 7 (2017) 5669–5678.
[40] J. Wang, G. Liu, T. Li, C. Zhou, Physicochemical studies toward the removal of Zn(II) and Pb(II) ions through adsorption on montmorillonite-supported zero-valent iron nanoparticles, RSC Adv., 5 (2015) 29859–29871.
[41] R.M.M. dos Santos, R.G.L. Gonçalves, V.R.L. Constantino, C.V. Santilli, P.D. Borges, J. Tronto, F.G. Pinto, Adsorption of Acid Yellow 42 dye on calcined layered double hydroxide: effect of time, concentration, pH and temperature, Appl. Clay Sci., 140 (2017) 132–139.
[42] Q. Cui, G. Jiao, J. Zheng, T. Wang, G. Wu, G. Li, Synthesis of a novel magnetic *Caragana korshinskii* biochar/Mg–Al layered double hydroxide composite and its strong adsorption of phosphate in aqueous solutions, RSC Adv., 9 (2019) 18641–18651.
[43] K. Kadirvelu, J. Goel, C. Rajagopal, Sorption of lead, mercury and cadmium ions in multi-component system using carbon aerogel as adsorbent, J. Hazard. Mater., 153 (2008) 502–507.
[44] R. Aziam, M. Chiban, H. Eddaoudi, A. Soudani, M. Zerbet, F. Sinan, Kinetic modeling, equilibrium isotherm and thermodynamic studies on a batch adsorption of anionic dye onto eco-friendly dried *Carpobrotus edulis* plant, Eur. Phys. J. Spec. Top., 226 (2017) 977–992.
[45] A. Proctor, J.F. Toro-Vazquez, The Freundlich isotherm in studying adsorption in oil processing, J. Am. Oil Chem. Soc., 73 (1996) 1627–1633.
[46] H.N. Tran, S.J. You, A. Hosseini-Bandegharaei, H.P. Chao, Mistakes and inconsistencies regarding adsorption of contaminants from aqueous solutions: a critical review, Water Res., 120 (2017) 88–116.
[47] N. Ayawei, A.N. Ebelegi, D. Wankasi, Modelling and interpretation of adsorption isotherms, J. Chem., 2017 (2017) 1–11.
[48] J. Poch, I. Villaescusa, Orthogonal distance regression: a good alternative to least squares for modeling sorption data, J. Chem. Eng. Data, 57 (2012) 490–499.
[49] K.Y. Foo, B.H. Hameed, Insights into the modeling of adsorption isotherm systems, Chem. Eng. J., 156 (2010) 2–10.
[50] S. Banerjee, M.C. Chattopadhyaya, Adsorption characteristics for the removal of a toxic dye, tartrazine from aqueous solutions by a low cost agricultural by-product, Arabian J. Chem., 10 (2017) S1629–S1638.
[51] A. Naskar, A.K. Guha, M. Mukherjee, L. Ray, Adsorption of nickel onto *Bacillus cereus* M^1_{16}: a mechanistic approach, Sep. Sci. Technol., 51 (2016) 427–438.
[52] R. Majumder, L. Sheikh, A. Naskar, Vineeta, M. Mukherjee, S. Tripathy, Depletion of Cr(VI) from aqueous solution by heat dried biomass of a newly isolated fungus *Arthrinium malaysianum*: a mechanistic approach, Sci. Rep., 7 (2017) 1–15.
[53] B. Subramanyam, A. Das, Linearized and non-linearized isotherm models comparative study on adsorption of aqueous phenol solution in soil, Int. J. Environ. Sci. Technol., 6 (2009) 633–640.
[54] P. Srivastava, S.H. Hasan, Biomass of mucorheimalis for the biosorption of cadmium from aqueous solutions: equilibrium and kinetic studies, BioResources, 6 (2011) 3656–3675.
[55] M. Butnariu, P. Negrea, L. Lupa, M. Ciopec, A. Negrea, M. Pentea, I. Sarac, I. Samfira, Remediation of rare earth element pollutants by sorption process using organic natural sorbents, Int. J. Environ. Res. Public Health, 12 (2015) 11278–11287.
[56] A.K. Meena, K. Kadirvelu, G.K. Mishra, C. Rajagopal, P.N. Nagar, Adsorptive removal of heavy metals from aqueous solution by treated sawdust (*Acacia arabica*), J. Hazard. Mater., 150 (2008) 604–611.
[57] S. Milonjic, A consideration of the correct calculation of thermodynamic parameters of adsorption, J. Serb. Chem. Soc., 72 (2007) 1363–1367.
[58] A. Sarı, M. Tuzen, D. Cıtak, M. Soylak, Adsorption characteristics of Cu(II) and Pb(II) onto expanded perlite from aqueous solution, J. Hazard. Mater., 148 (2007) 387–394.
[59] Y. Shen, X. Zhao, X. Zhang, S. Li, D. Liu, L. Fan, Removal of Cu^{2+} from the aqueous solution by tartrate-intercalated layered double hydroxide, Desal. Wat. Treat., 57 (2016) 2064–2072.